ADVANCED FUNCTIONAL MATERIALS
www.afm-journal.de

Materials Views
www.MaterialsViews.com

Random Lasing in Self-Assembled Dye-Doped Latex Nanoparticles: Packing Density Effects

Luis Cerdán, Angel Costela, Eduardo Enciso, and Inmaculada García-Moreno*

Efficient random lasing (RL) from self-assembled dye-doped latex nanoparticles ($d = 50–380$ nm) presenting size polydispersity is reported. This new system exhibits a very good chemical compatibility between dye (Rhodamine 6G) and polymer as well as a high refractive index contrast between nanoparticle and surroundings (air), in such a way that its emission properties surpass the ones previously reported in similar systems. Furthermore, this system allows analyzing in detail the effects of the nanoparticle size polydispersity and the packing density on the RL emission properties. It is shown that size polydispersity gives rise to non-uniformities in the filling fraction along the sample that lead to fluctuations on the scattering length across the sample and thus to a variation on the emission properties. Finally, it is observed that the increase of the filling fraction, enabled by the use of binary mixtures of nanoparticles with different sizes, results in remarkable improvements in the RL emission properties.

1. Introduction

In a gain medium with a randomly distributed refractive index, light is both multiply scattered and amplified, giving place to the so-called random lasing (RL).[1] Given their particular laser properties, these media have been the subject of extensive research, mostly in the last decade since the discovery of coherent RL in semiconductor powders by Cao et al.[2] RL has been observed in many different materials and configurations such as dye solutions incorporating passive[3–5] or plasmonic[6] scatterers, semiconductor powders,[2,7] laser crystal powders,[7] photonic amorphous structures,[8] disordered photonic crystal waveguides,[9] fibers and slab waveguides with naturally occurring defects[10,11] and thin films with induced heterogeneities,[12,13] among many others. In this regard, photonic glasses, formed by randomly self-assembled monodispersed spherical active[14] or passive[15–18] (embedded in an active medium) micro/nanoparticles, have recently attracted interest due to the possibility to tailor their RL emission properties by modifying the nanoparticle size.

Our group has recently developed new dye-sensitized organic nanoparticles (NP) based on latexes. We have demonstrated significant improvements in the lasing efficiency and photostability of dye Rhodamine 6G (Rh6G) and mixtures of dyes undergoing energy transfer by confining the dyes into polymeric NPs (latexes) homogeneously dispersed in aqueous colloidal suspensions.[19–21] In the latest work,[21] the colloidal suspensions were left to dry and solid samples of self-assembled NPs were obtained, enabling the first demonstration of energy transfer assisted incoherent RL from solid samples of dye-doped latex NPs. Furthermore, another benefit of this system, with respect to those reported before, is that the dye is embedded inside the NPs and there is no need to infiltrate the obtained self-assembled solid with an active medium,[17,18] whereupon the system presents a high refractive index contrast between NP and surroundings (air), thereby compensating the reduced size of the NPs.

It is well known that the scatterer size affects drastically the RL emission properties.[22] Less consideration has been given to the weight of the polydispersity in these properties, albeit it is known that the size polydispersity washes-out the Mie resonances[18] and affects the filling fraction.[23] In fact, the characteristic length scales that determine the light transport and RL emission properties in these systems are the scattering mean free path l_{sc}, defined as the average distance the light must travel between two consecutive scattering events, and the transport length l_t (or transport mean free path), defined as the average distance a wave must travel before its direction of propagation is randomized. The calculation of the scattering length is relatively easy when the scatterers are spherical and the scattering is weak (particle-particle interaction vanishes) because[14]

$$l_{sc}(\omega) = \frac{1}{\rho\sigma_{sc}(\omega)} = \frac{4\pi r^3}{3\phi\sigma_{sc}(\omega)} \quad (1)$$

where ρ is the density of scatterers, $\sigma_{sc}(\omega)$ is the frequency-dependent scattering cross section, r is the scatterer radius and ϕ is the volume filling fraction, which depends strongly on the size polydispersity.[23] On the other hand, l_{sc} and l_t are related by[14]

Dr. L. Cerdán, Prof. A. Costela,
Prof. I. García-Moreno
Instituto de Química Física "Rocasolano"
Consejo Superior de Investigaciones Científicas (CSIC)
Serrano 119, 28006, Madrid, Spain
E-mail: lcerdan@iqfr.csic.es
Prof. E. Enciso
Facultad de Ciencias Químicas
Universidad Complutense de Madrid (UCM)
Av. Complutense s/n, 28040, Madrid, Spain

DOI: 10.1002/adfm.201202616

$$l_t(\omega) = \frac{l_{sc}(\omega)}{1 - \langle \cos\theta(\omega) \rangle} \quad (2)$$

where <cos θ (ω)> is the average cosine of the scattering angle, which can be found from the differential scattering cross section.

A quick inspection of Equations (1) and (2) reveals the relative weight on the transport length of both the scatterer size and the filling fraction. It can be shown[14] that for weak scattering $l_t \propto r^{-3}$, whereas the filling fraction variation affects as $l_t \propto \phi^{-1}$. Hence, the effect of varying the scatterer size is much more drastic that the variation with the filling fraction, which explains why the RL emission properties are the most of the times assessed as a function of the scatterer size and why the filling fraction effects are left apart. Nevertheless, its influence cannot be neglected and merits to be studied more profoundly. In relation with this, the NPs synthesized in our lab present certain degree of size polydispersity which, in view of the existing correlation between this and the filling fraction, enables to inquire on the effects of the filling fraction in the RL properties of the self-assembled solids.

In this paper we report a study on the structural and RL emission properties of self-assembled dye-doped NPs of different sizes (d = 50–380 nm) presenting size polydispersity. We first perform a structural characterization of the synthesized latexes and the dried solid samples obtained from them, follow by an assessment of the emission properties evaluated as a function of NP size and sample position. Finally, we assess the variation of the emission properties when modifying the filling fraction of the samples in a controlled way.

2. Structural Characterization of Latexes and Samples

2.1. Size Distribution

The NP size is mainly determined by the surfactant concentration (**Table 1** and **Figure 1**a), but can be slightly affected by the addition of dye.[20] The NP diameter, as measured by dynamic light scattering (DLS), is larger than the diameter obtained by scanning electron microscopy (SEM) images by an average factor of 1.2, since the hydrodynamic radius of the NP in the suspension is increased, with respect to that of the dried NP, by means of water swelling in the hydrophilic 2-hydroxyethyl methacrylate (HEMA) portions of the polymer chains. At large surfactant concentrations, always below the critical micelle concentration (CMC) value of aqueous solution (≈8×10^{-3} M), the number of stabilized nuclei increases, leading to smaller NP sizes at the end of the polymerization (Table 1 and Figure 1a). At low surfactant concentrations the NP diameter grows as a consequence of the incorporation of polymer chains to the emergent particle, so that enough sulfate groups can stabilize the suspension.

On the other hand, the NP size polydispersity rises for suspensions with low and large amounts of surfactant. In the former case, and following the argument given above, the NP nuclei coalesce until they become stable against collisions. If the surfactant concentration is too large, it stabilizes initial NP nuclei of different sizes, which results in the broadening of the final NP size distribution. Under the selected experimental conditions, only intermediate surfactant concentrations leads to highly monodispersed NPs (polydispersity ratio PDR < 0.05, see Table 1), and the drying of these suspensions results, in some

Table 1. Surfactant effects on the synthesis of poly(MMA-HEMA) NPs at 65 °C, with 0.28 wt% (with respect to the amount of monomer) of Rh6G.

Sample	[SDS] [10^{-3} M]	Polymerization yield [%]	NP diameter[a] [nm]	σ[b]	PDR[c]	φ[d]
MH1	6.7	75	51	0.245	0.062	–
MH2	3.6	72	59	0.219	0.049	–
MH3	2.3	79	77	0.225	0.068	0.71
MH4	1.9	81	87	0.191	0.037	0.66
MH5	1.5	68	97 [76]	0.141	0.02	–
MH6	1.2	78	119 [96]	0.157	0.025	0.61
MH7	0.81	73	167 [136]	0.183	0.034	0.62
MH8	0.63	72	215 [180]	0.183	0.034	–
MH9	0.42	73	380 [306]	0.251	0.065	–

[a]Estimated by DLS; value in brackets is diameter estimated from SEM pictures; [b]Standard deviation of log-normal size distribution estimated by DLS; [c]Polydispersity ratio (PDR), $\sigma^2 = \ln(1+PDR)$; [d]Filling fraction.

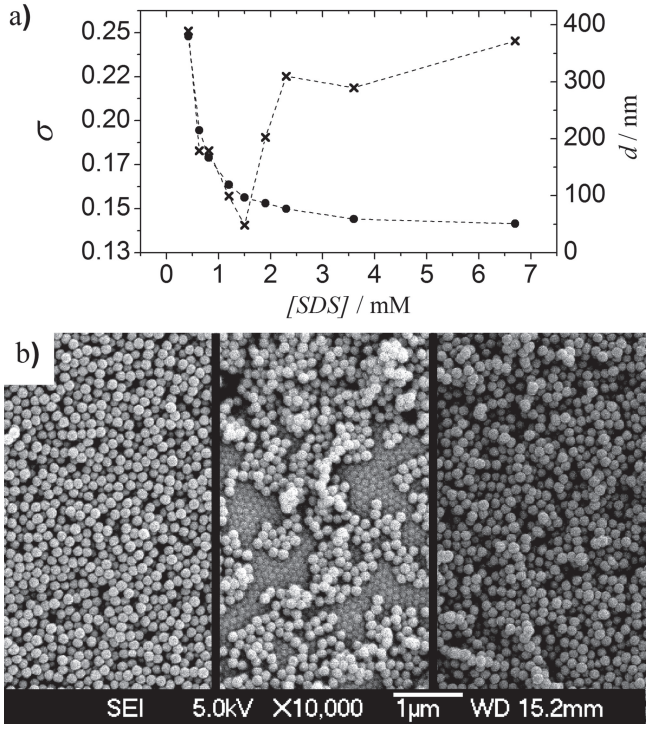

Figure 1. a) Nanoparticle size d (filled circles) and polydispersity σ (crosses) as a function of surfactant concentration; b) SEM images of different pieces of sample MH7.

cases, in ordered domains, as can be nicely appreciated in the SEM images of Figure 1b.

2.2. Structural Properties of Self-Assembled Solid Samples

After drying the suspensions, either at room temperature or at 40 °C, solids with different densities are formed, depending on the degree and type of NP packing. The size polydispersity and the loss of NP stabilization give place, after drying, to local inhomogeneities in the filling fraction across the sample, i.e., each part of the sample has a different NP random arrangement.[24] This variety of arrangements is nicely depicted in Figure 1b, which shows SEM images for different areas of the sample MH7 (low polydispersity), all of them showing a random NP arrangement with a, seemingly, different degree of packing. But the most remarkable fact in these pictures is that there are local regions which even present a crystalline phase partially covered by an amorphous phase, as can be clearly observed in the central image. Nevertheless, the crystalline phase is residual, as revealed when analyzing several SEM images (Supporting Information Figure S1-S3) and confirmed by nitrogen adsorption isotherms (see below and Supporting Information). The quantitative characterization of the relative amount of each particle ordering in the latex monoliths would require a costly SAXS experiment,[24] but this degree of accuracy is beyond the scope of the present work.

Thanks to the submicrometric nature of the NPs, the external surface and the volume of the interparticle voids present in most of the solid samples can be characterized from nitrogen adsorption isotherms. All the measured isotherms exhibit a typical type-IV curve[25] (Supporting Information Figure S4a) and broad pore size distributions (Supporting Information Figure S4b). These features indicate the occurrence of multilayer adsorption at low pressures and nitrogen condensation inside the matrix pores, as observed by the enhancement of nitrogen adsorption at reduced pressures larger than $P/P_0 = 0.4$.[25] In addition, the hysteresis (Supporting Information Figure S4a) reveals the presence of small pores which origin is found in the three particle contact voids that block the nitrogen exit from some large pores. It is worth bringing the attention to the absence of any structure in the pore size distributions (Supporting Information Figure S5), a fact that reveals the absence of NP ordering in the solid samples,[26] in agreement with a photonic glass structure (see Supporting Information).

On the other hand, the ratio of free specific NP surface (A_{th}) to Brunauer-Emmett-Teller (BET) area[25] (A_{BET}) is seen to increase for small NP diameters (Supporting Information Table S1), fact that can be ascribed to both a higher coalescence between NPs and the presence of residual surfactant in those solid samples. Furthermore, the measured mesopore volumes increase with the NP diameter, reaching a maximum value for the sample MH6, and decreasing when the amorphous solid samples show voids which sizes are outside the experimental window of this technique (diameters beyond approximately 150 nm). According to this limitation, the measured pore volumes of sample MH8 should be considered as a lower limit of the actual pore volume.

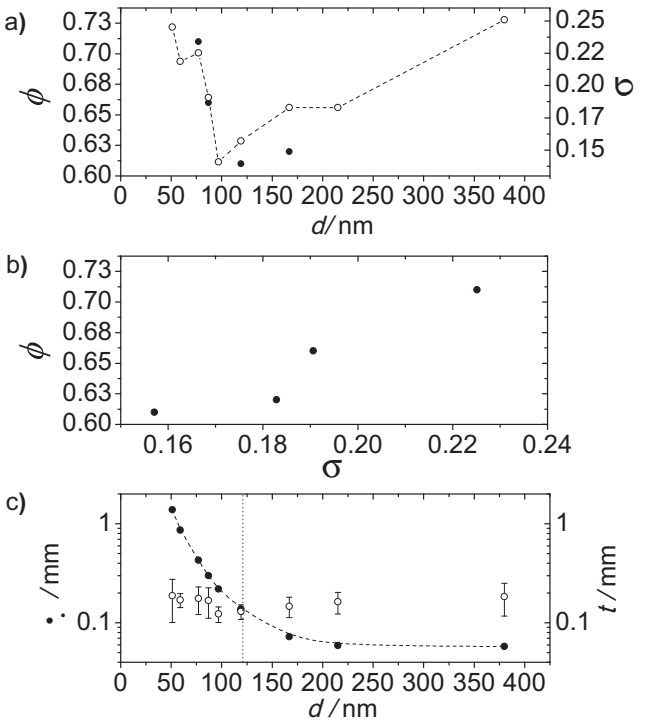

Figure 2. a) Filling fraction φ (filled circles) and polydispersity σ (hollow circles) as a function of NPs size (d). b) Dependence of filling fraction on polydispersity. c) Transport length at 580 nm (filled circles) and sample thickness t (hollow circles) as a function of NP size (d). The dotted line in (c) marks the boundary between diffusive and sub-diffusive transport regimes.

From the pore volumes the filling fraction (φ) of the solids can be estimated as $\phi = V_p/(V_p + V_{mesopore})$, where V_p and $V_{mesopore}$ are the specific NP and pore volumes, respectively (see Supporting Information Table S2). The estimated filling fraction values are depicted in **Figure 2**a as a function of the NP size. φ is maximized for the NPs with the lowest sizes, reaches a minimum for NPs ≈ 100 nm in size, and grows again for the highest NPs. Although the results showed in Figure 2a have to be understood as demonstrating a qualitative tendency, this behavior is very similar to the one exhibited by the polydispersity when assessed as a function of NPs size (Figure 2a) in agreement with the correlation between polydispersity and filling fraction demonstrated by Farr and Groot[23] and experimentally observed in the present work (Figure 2b). It is worth noticing that the filling fraction values estimated for the smallest NPs must be taken with care. When the solid content of the suspensions raises due to water evaporation, the concentration of surfactant increases, reducing the electrostatic stabilization of the suspension and allowing the aggregation of NPs after collision. Such aggregation is facilitated by the swelled nature of the HEMA monomers present in the NP surface. Not in vain, we have observed the formation of gels by water evaporation in those systems. As a consequence, after drying the suspensions with larger amounts of surfactant (small NPs), the NP aggregation leads to a denser amorphous structure. In addition, once the samples are dried, the surfactant can be trapped in the

inter-particle interstices, contributing to the free space occupation and reducing the BET area, which in turn leads to higher filling fractions. For this reason the nitrogen isotherms of samples MH1 and MH2 have not been measured.

3. Random Laser Emission

In RL two different operational regimes may be distinguished, incoherent RL and coherent RL. On the one hand, Incoherent RLs, in which there is only intensity or energy feedback,[27] show a smooth spectral shape characteristic of amplified spontaneous emission (ASE) reinforced by the enlarged optical path induced by the scattering. On the other hand, coherent RLs, in which there is field or amplitude feedback,[27] present similar ASE spectra but superimposed with multiple very narrow spikes associated with spatially extended lasing modes.[28]

From the NPs size and the estimated filling fraction one may obtain the transport length by making use of Mie scattering calculations (assuming $n_{NP} \approx 1.5$; $\lambda = 580$ nm; $\varphi = 0.62$).[29] The computed results, depicted in Figure 2c, show that the higher the NP size is, the shorter the transport length becomes, as expected.[14,18,30] When comparing this value with the sample thickness t (Figure 2c) one observes that as the NP size increases there is a transition from the sub-diffussive, or ballistic, transport ($l_t > t$) to the diffusive transport ($l_t < t$).[22] This, together with the fact that in our system $kl_t = 630$–$15\,000$, with $k = 2\pi/\lambda$ and $\lambda = 580$ nm, suggests that this system will operate in the incoherent regime, unless very high pump intensities are used.[28,31]

In order to assess this extent we performed a quick inspection of the emission spectra when pumped above laser threshold. **Figure 3**a shows the normalized photoluminescence (PL) spectrum of the colloidal suspension of Rh6G doped NPs before drying and the RL spectrum of the dried sample MH5 (d = 97 nm) excited at different pump intensities below and above threshold. The lack of spikes over all of the RL spectra suggests that this system operates in the incoherent regime, even for the highest pump intensities used in the present work (490 kW cm^{-2}). Nevertheless, at this pump intensity some of the samples presented incipient coherent RL spectral features, indicating that probably this regime was reached, albeit not entirely crossed. Higher pump intensities could not be used in order to explore the excitation of coherent RL since a clear and distinctive irreversible dye photobleaching did appear in the samples after just a few pump pulses when pumping above 500 kW cm^{-2}.

It is worth pointing out at this point that previous photophysical studies[20] showed that these NPs do not present neither dye aggregation nor quenching effects, even at the high dye loadings used (6.7 mM) within the NPs.

3.1. Variation of RL Properties with NP Size

The samples were subjected to systematic studies on the RL emission properties as a function of excitation intensity. From the emission spectra one can retrieve valuable information such as the output relative intensity integrated over the whole spectral range, the relative peak intensity, the peak wavelength and the full width at half maximum (FWHM). In addition, from the light-light curve (Figure 3b) it is possible to obtain the RL threshold intensity, a parameter of utmost importance in RLs. The RL threshold is considered to be the point for which there is a change in slope in the light-light curve when plot in a log-log scale (Figure 3b) or normal scale (Figure 3c). The change in slope in the light-light curve at RL threshold is not very significant in these samples (Figure 3b,c), since in the incoherent regime the RL emission behavior resembles that of amplified spontaneous emission,[7] which is known to present smooth transitions at threshold.

It is worth noticing that at this point the FWHM of the output spectrum is half the fluorescence FWHM (Figure 3b). In fact, this criterion has been used in the past to estimate the threshold intensities in the frame of ASE research.[32,33]

On the other hand, our samples present non-uniformities (Figure 1b) that lead to fluctuations of the scattering length across the sample. Hence, in order to evaluate this induced

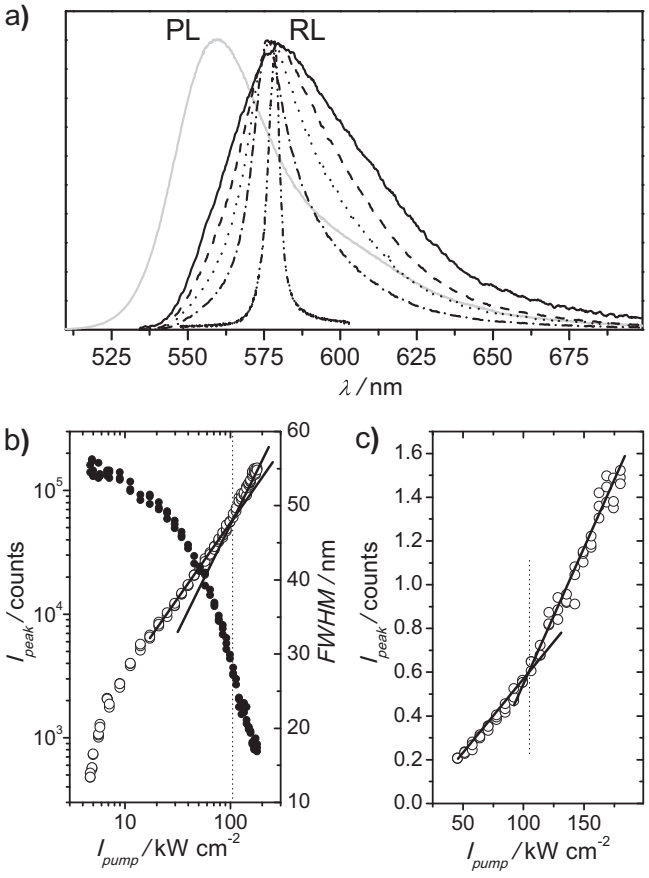

Figure 3. a) Normalized photoluminescence (PL, gray solid line) spectrum and random laser (RL) emission spectra of sample MH5 (d = 97 nm) pumped at 7 kW cm^{-2} (solid line), 50 kW cm^{-2} (dashed line), 100 kW cm^{-2} (dotted line), 180 kW cm^{-2} (dash-dot line) and 490 kW cm^{-2} (dash-dot-dot line). b) Light-light curve in log-log scale (hollow circles) and FWHM (filled circles) as a function of pump intensity for sample MH5. c) Close-up view of light-light curve in b) around RL threshold region in linear scale. The solid lines are a guide to the eye, and the dotted lines mark the RL threshold position.

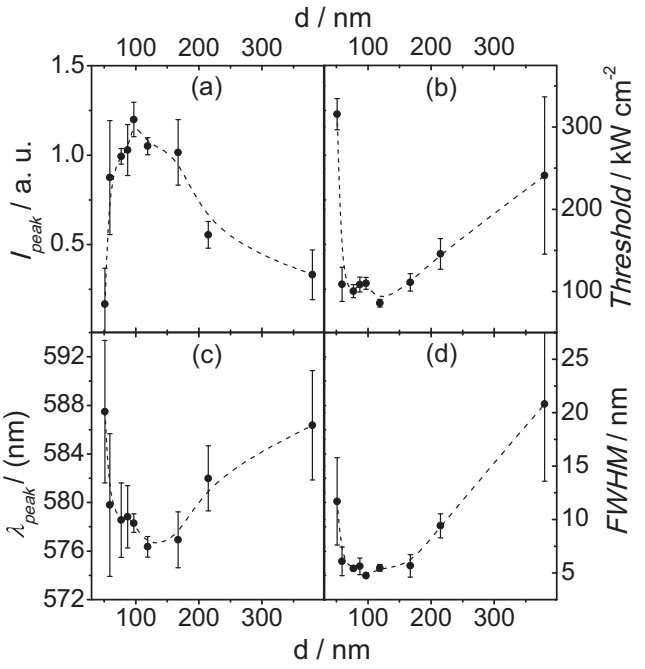

Figure 4. Variation of a) emission peak intensity (I_{peak}), b) threshold intensity, c) peak wavelength (λ_{peak}) and d) FWHM as a function of NP size. Each point and error bar represents the average and standard deviation, respectively, over five acquisitions on different sample positions. Data in (a,c,d) acquired at an excitation intensity 490 kW cm^{-2}. Dashed lines are guides to the eye obtained with a b-spline interpolation of the average values.

inhomogeneity, and to study the subsequent filling fraction effects on the RL properties, the emission spectra were recorded in different positions (pieces) of the same sample.

Figure 4 shows a clear dependence of the emission parameters on both the NPs size and sample position when pumped well-above threshold (490 kW cm^{-2}). The average peak intensity (Figure 4a) rises abruptly as the NP size is increased, reaching an emission maximum for NPs close to 100 nm in size ($l_t \approx$ 220 μm). For NPs larger than this value (shorter transport lengths), the emission intensity is abruptly reduced. The very same behaviour, which can be ascribed to geometrical effects due to the pumping configuration,[34] has been observed and predicted in the past for different active scattering media in this range of transport lengths.[34,35] The change in the average output peak emission is translated, as expected, in an opposite change on the average laser threshold (I_{th}), i.e., the higher the peak intensity is, the lower the threshold becomes, as is depicted in Figure 4b. These results show that the transport lengths attained in the present work are not short enough as to enter the regime for which $I_{th} \propto l_t^{0.5}$,[22] indicating that we are far from RL with resonant feedback, as has been observed already. In addition, this particular system presents quite low RL thresholds, most probably due to the simultaneous combination of a high gain material (Rh6G dye), a high refractive index contrast between NP and surroundings, and a large excitation area, which is known to reduce the RL threshold.[7,18,22] It is worth noticing that, even presenting larger transport lengths than in ref. [17,18] the RL threshold values in our system (90 kW cm^{-2} or 1.6 mJ cm^{-2}) are lower than, or comparable to, the ones reported in ref. [17] (640 mJ cm^{-2}; polystyrene NPs infiltrated with DCM/DNA) and ref. [18] (1.75 mJ cm^{-2}; SiO_2 NPs infiltrated with BBEHP-PPV and considering a pump area 0.1 cm^2, as in our work).

A similar trend is found for the peak wavelength (Figure 4c), which is blue-shifted as the transport length is reduced, reaching a maximum blue-shift (λ_{peak} = 576 nm) at $l_t \approx$ 140 μm (NPs with diameters between 100 and 125 nm), and red-shifting again for shorter transport lengths. Finally, the FWHM (Figure 4d) reaches a minimum of 5 nm for NPs 100 nm in diameter. A similar behavior has been observed before in dye solutions containing passive scatterers.[31] The dependence of the FWHM on the NP size indicates that the degree of amplification is maximum for NPs 100–125 nm in size ($l_t \approx$ 140–220 μm) and is reduced for larger and smaller NPs, much in agreement with the results on the peak and threshold intensities.

It is quite remarkable the variation on the emission properties when measured in different sample positions (error bars in Figure 4). As mentioned above, this variability has its origin on the NPs size polydispersity and the loss of NP stability when the surfactant concentration increases in the drying process, which give place to local inhomogeneities in the filling fraction across the sample, or what is the same thing, each part of the sample has a different NPs random arrangement (Figure 1b) and even a different size distribution which, consequently, gives place to different scattering environments and transport lengths. These results show that in RL based on self-assembled NPs, the size polydispersity effects cannot be neglected.

In this sense, the lower the polydispersity is, the lower the RL properties variability becomes (more homogeneous sample), with the lowest polydispersity and variability being obtained for the sample with NPs 100 nm in size (Figure 2a and Figure 4). In conclusion, the average RL properties are determined by the NP size, whereas the polydispersity mainly contributes to the observed variability through its influence on the filling fraction and thus on the transport length.

3.2. Variation of RL Properties with Packing Density (Filling Fraction)

To experimentally assess the sole effects of the filling fraction on the RL emission properties, it would be necessary to manage varying that fraction without changing the other variables, i.e., NP size and polydispersity. Fortunately, there are different ways in which this goal may be attained. It has been recently shown[15,16] that self-assembled NPs with increased disorder, and thus reduced filling fraction, can be obtained by dissolving in the colloidal suspension controlled amounts of ions to provoke colloidal flocculation, giving place to the so-called photonic glasses. Photonic glasses infiltrated with organic emitters have been successfully used to tune in a controlled way the emission peak in random lasers[17,18].

We have used this strategy to change in a controlled way the filling fraction and to assess its effects on the RL emission properties for the sample MH8, which presents one of the lowest transport lengths ($l_t \approx$ 60 μm) and a moderate polydispersity

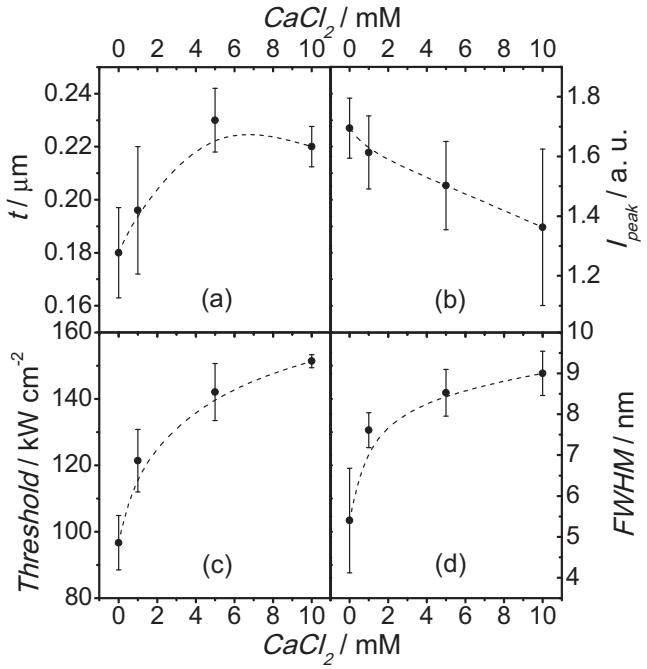

Figure 5. Dependence on $CaCl_2$ concentration of a) sample thickness, b) emission peak intensity (I_{peak}), c) RL threshold intensity and d) FWHM. Each point and error bar represents the average and standard deviation, respectively, over five acquisitions on different sample positions. Data in (b,d) acquired at an excitation intensity 490 kW cm^{-2}. Dashed lines are guides to the eye obtained with a b-spline interpolation of the average values.

($\sigma \approx 0.183$). **Figure 5**a shows that the addition of $CaCl_2$ in small amounts gives place to ≈20% increase in the sample thickness, which is a direct consequence of the decrease (of ≈20%) in the filling fraction. The reduction in the filling fraction is translated into an increased transport length (Equation 1) and leads to a non-vanishing decrease in the peak intensity, a remarkable increase in the threshold one and a large broadening of the FWHM, as can be observed in Figure 5b,c,d, respectively. One might reason that the observed RL emission properties variation is due to the change in the sample thickness. Nevertheless, this is not the case in sample MH8, since the minimum thickness is ≈180 micrometers, whereas the pump light is absorbed in e^1 in just 25 µm (Mie calculations[29]), i.e., the emission and scattering processes only happens "superficially". In other words, the sample could be considered as a semi-infinite plane for the RL process.

These results show that the observed variability in the emission properties represented in Figure 4 is fully compatible with the assumption on the appearance of local inhomogeneities across the sample, which leads to changes in the filling fraction and thus in the transport length.

As a final remark, we observed that if the samples were dried at 40 °C in an oven instead of at room temperature, there was no need to add salt to increase the disorder and to reduce the filling fraction in our samples. By increasing the drying temperature the evaporation time is reduced in such a way that the NPs are self-assembled forming a more disordered structure. The influence on the RL emission properties (not shown) is analogous to that of the addition of salt, i.e., the peak intensity is reduced, the RL threshold intensity is increased, the emission wavelength is red-shifted and the FWHM is slightly reduced. Nevertheless, the influence of the drying temperature is not as strong as the influence of the salt addition.

Up to here we have seen that the decrease of the NP packing leads to a worsening of the emission properties. Then, a priori, the increase of the former (increase in the filling fraction) should result in an improvement of the later. According to ref. [[23]] it is possible to increase the filling fraction of randomly close packed hard spheres by reducing the fluid viscosity or by increasing the size polydispersity. Neither of these options is possible with our systems and we have been unable to find a way to increase the filling fraction while leaving the NP size fixed. Nevertheless, there is an alternative approach to increase dramatically the filling fraction of self-assembled NPs by making use of binary mixtures of NPs of different sizes. According to the results shown in ref. [[23]], the more different the NP sizes are, the higher the achievable filling fraction is, with a limit as high as 0.88.

Following this route we began by mixing NPs with the highest size ratio available in our samples, this is, MH1 (d_1 = 51 nm) and MH9 (d_2 = 380 nm), which results in a ratio $R = d_1/d_2 = 7.5$. Unfortunately, in the drying process a clear phase separation appeared between both types of NPs, with the MH9 NPs decanting to the bottom and the MH1 NPs laying on top of the MH9 NPs. This phase separation gave place to shear stress, resulting in the bending of the solid sample pieces. Both facts made the obtained samples useless. We made some more attempts and found that a good compromise between sample quality and size ratio was provided by samples MH4 (d_1 = 87 nm) and MH7 (d_2 = 167 nm), which results in a ratio $R = d_1/d_2 = 1.9$, high enough as to increase substantially the filling fraction.[23] The most interesting point is that both samples present very similar RL emission properties by themselves (Figure 4), with the MH4 sample surpassing somewhat the MH7 one, which makes this system the perfect bench to see whether synergy emerges when following the binary mixture approach.

Figure 6 depicts the RL emission properties as a function of the weight percentage of smaller NPs (MH4) in the final sample. As the amount of MH7 is increased up to a 25%, the emission efficiency is improved, with an increase in the peak intensity, a reduction in the threshold intensity and a collapse in the spectral FWHM. Once the MH7 weight proportion surpasses a 25% the emission efficiency is lowered monotonically until a 100 MH7 wt% is reached, when the emission properties of the sample MH7 are recovered. The improvement in RL properties when changing the MH7 weight proportion can be mirrored as well in the evolution of the RL emission spectra plotted in Figure 6d. These results clearly show that the binary mixtures can improve significantly the RL emission properties of the mixture constituents when operated separately.

Figure 7a shows that the binary mixtures present larger filling fractions, with the maximum at 25 wt% MH7, than the ones corresponding to the mixture constituents by themselves. This fact can be observed as well in the SEM images in Figure 7b. This last result backs up the idea that the increase of the NP

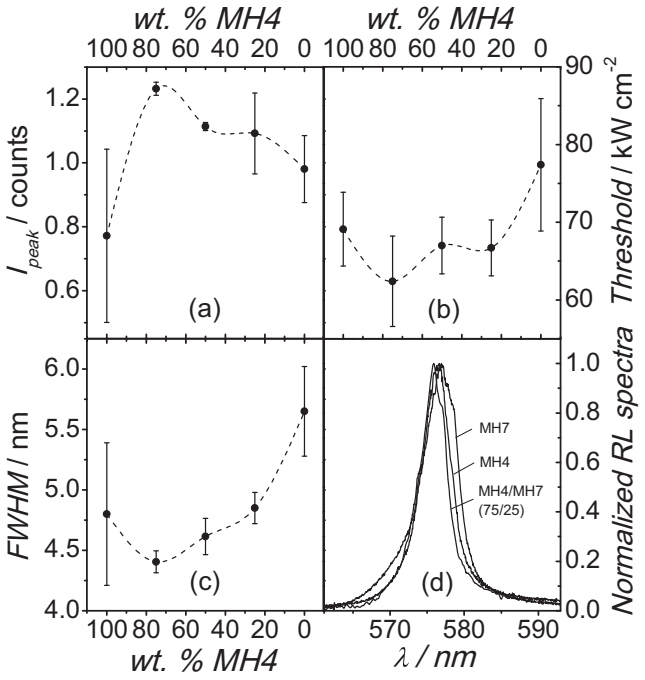

Figure 6. Dependence on MH4 wt% of a) emission peak intensity (I_{peak}), b) RL threshold intensity, and c) FWHM. d) RL emission spectra of samples MH4, MH4/MH7 (75 wt% MH4) and MH7. Each point and error bar in (a–c) represent the average and standard deviation, respectively, over five acquisitions on different sample positions. Data in (a,c,d) acquired at an excitation intensity 490 kW cm^{-2}. Dashed lines in (a–c) are guides to the eye obtained with a b-spline interpolation of the average values.

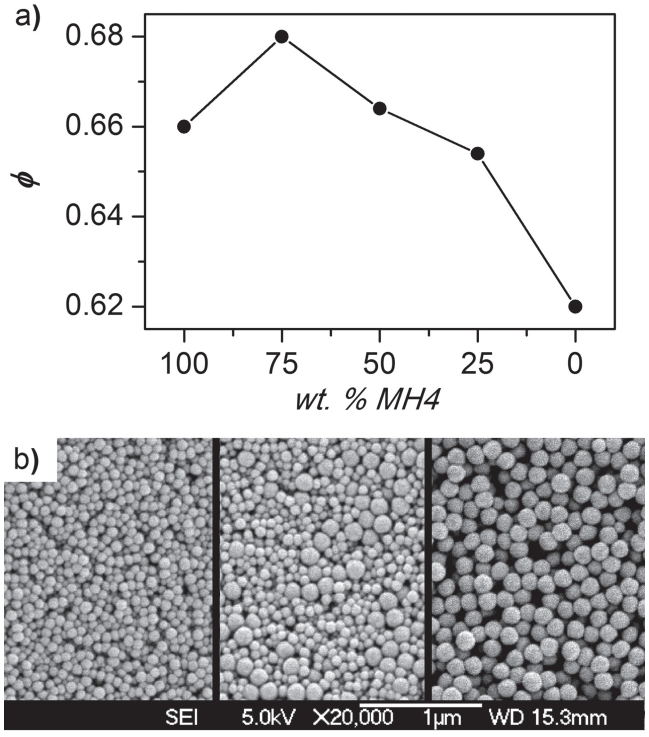

Figure 7. a) Variation of filling fraction as a function of MH4 wt%. b) SEM images of samples MH4, MH4/MH7 (75 wt% MH4) and MH7.

packing density (increase in the filling fraction) leads to an improvement of the emission properties.

As a final remark on the binary mixtures structural properties, one could expect a homogeneous mixture in which the large NPs would be separated from each other and surrounded by the smaller ones. The SEM images in Figure 7b shows that, on the contrary, the binary mixture is heterogeneous, with clusters of large NPs (groups of 3 to 6 NPs) surrounded by small NPs.

4. Conclusion

We have presented in this paper a study on the random lasing properties of randomly self-assembled dye-doped NPs presenting size polydispersity. We have demonstrated that this system operates in the incoherent regime, since there is a lack of spectral spikes whatever the pump intensity is. The emission properties have been observed to strongly depend on the NPs size and the filling fraction, presenting the lowest RL thresholds (90 kW cm^{-2}) and minimum FWHM (5 nm) for samples with intermediate size (120 nm) and low PDR (0.02), being that threshold value lower, or comparable to, the ones reported in other works, most probably due to the simultaneous combination of a high gain material (Rh6G dye) and a high refractive index contrast between NP and surroundings. We have observed that the reduction of the filling fraction in the dried samples, by adding salt to force flocculation or rising the drying temperature, is deleterious to the RL emission properties. On the other hand, we have been able to increase the filling fraction of the dried samples by making use of binary mixtures of NPs with different sizes, which has given place to a remarkable improvement in the RL emission properties. In conclusion, we have observed that the size polydispersity gives place to non-uniformities in the filling fraction along the sample that leads to emission variability through the sample, but this polydispersity can increase at the same time the filling fraction, which is beneficial for the final RL emission properties.

5. Experimental Section

Materials: Methyl methacrylate (MMA) (Aldrich, 99%) was purified with a 0.1 M sodium hydroxide solution to remove inhibitor. 2-Hydroxylethyl methacrylate (HEMA) (Aldrich, 97%), potassium persulfate (KPS) (Sigma, 99%), Rhodamine 6G (Rh6G) (Fluka) and sodium dodecyl sulphate (SDS) (Sigma 99%) were used without further purification. Deionized water was obtained from a Direct Q 5 Millipore.

Synthesis of Nanoparticles: Rh6G doped polymeric NPs were prepared from a batch emulsion polymerization of MMA.[20] Taking into account that the laser action of xanthene dyes is enhanced in protic but not very polar media,[36,37] the original recipe from Nagao et al.[38] was modified by copolymerizing the hydrophobic monomer MMA with a more hydrophilic one such as HEMA, introducing in the monomer mixture feed a weight ratio of those monomers as 80:20. SDS was added into the feed mixture as colloidal surfactant stabilizer[39] in order to stabilize large number of NP nuclei and, as a consequence, to control the final NP diameter. Since the SDS employed concentration was always below the critical micelle concentration (CMC) in water (around 8×10^{-3} M), the monomer

polymerization occurs basically in the aqueous phase, until the oligomer concentration reaches the precipitation threshold, as it is characteristic in soap free emulsion polymerizations. The free radical polymerization was carried out at 65 °C with monomer content in the feed of 7.4 wt% related to the total mass in the suspension. The reaction was initiated by adding 0.8 wt%, with respect to the monomer present in the feed, of a water soluble initiator such as KPS. As it is shown in Table 1 high polymerization yields were obtained. All samples were prepared with a dye concentration of 0.28 wt% with respect to the feed monomer content. The monomer conversion was determined gravimetrically by removing aliquots after polymerization and drying them in the oven. The obtained dispersions, with a latex content around 5.5 wt%, were not cleaned, since the centrifugation leaded to aggregation, and dialysis produced a gel after several water changes. In terms of evaluating the effect of the SDS in the NP size different samples have been synthesized (see Table 1).

Particle Characterization: The morphology and microscopic structures of the latex solid samples were observed using field emission scanning electron microscopy (FESEM, JEOL, JSM-6700F) with an acceleration voltage of 5–10 kV and the emission current of 10 μA. The samples were fragments of solid samples obtained after drying the suspensions. The diameters of the NPs were measured by dynamic light scattering (DLS) with a 90Plus/BI-MAS equipment (BIC) and, when possible, from the SEM pictures.

Sample Preparation: The samples were obtained with a method analogue to the modified self-assembly method reported in ref. [16]. A poly-(methyl methacrylate) (PMMA) hollow cylinder with a height of h = 1 cm and inner radius 1 cm was fixed with impermeable silicone to a clean PMMA substrate. It was then filled with 2 mL of colloidal suspension with a 5 wt% of NPs previously prepared and the solution is left to dry at room temperature (or oven at 40 °C) until complete water evaporation. The wet NP amorphous monolith binds the substrate, and shear stress is generated that resist the solid sample shrinkage under water evaporation. If the magnitude of the stress exceeds a critical threshold, cracks appear originated in the multiple defects of the polydispersed NP arrangements.[40] Pieces from the center of the sample were selected to avoid meniscus effects in the sample edge, and were stuck to a microscope cover glass (2 cm × 2 cm) to allow sample manipulation. The thickness of the samples was measured by using a digital comparator (Mahr Extramess 2001) with a resolution of up to 0.2 μm. To perform the flocculation experiments solutions of $CaCl_2$ were added to the colloidal suspensions in such a way that the final salt concentration ranged from 1 mM to 10 mM.

Adsorption Isotherms: Nitrogen adsorption isotherms at 77 K were obtained with an ASAP 2020 equipment from Micromeritics. Prior to adsorption measurement, samples were outgassed at 50 °C for 10 h. Isotherms were analyzed with the BET equation and the standard t plot, which gave the BET area (A_{BET}) and the micropore volume (V_{mic}), respectively.[25] Pore size distributions were obtained by BJH analysis of the adsorption and desorption branches of the isotherms with the assumption of a cylindrical pore model.[25]

Laser Measurements: The solid samples were pumped at 532 nm with 20 ns FWHM pulses from a frequency-doubled Q-switched Nd:YAG laser (Lotis TII SL-2132) at 15 Hz repetition rate. The pump radiation was horizontally polarized, which allowed controlling the pulse energy incident on the sample by insertion into the pump beam path of a half-wave plate (HWP) and a linear polarizer (LP) set with its polarization axis horizontal. By rotating the HWP the linear polarization of the input beam is rotated out of the horizontal, and the pump beam is blocked more or less by the LP, depending on the rotation angle introduced by the HWP. The light incident on the sample was focalized onto the sample with a spherical quartz lens (f = 15 cm), at an angle of incidence of 34° with respect to the normal to the surface of the sample. The spot on the surface of the sample was elliptical with major and minor axis of 2 mm and 1.6 mm, respectively. The RL emission was collected normal to the sample with a 5-cm focal length spherical lens, focused onto a fiber bundle and detected with a spectrograph/monochromator equipped with a thermoelectrically cooled CCD detector. Neutral density filters were used to avoid CCD detector saturation. The integration time in the CCD was set at 1000 ms so that all the measurements were averaged over fifteen pulses.

Supporting Information

Supporting Information is available from the Wiley Online Library or from the author.

Acknowledgements

This work was supported by Projects TRACE2009-0144 and MAT2010-20646-C04-01 of the Spanish Ministerio de Economía y Competitividad (MINECO). Also, Universidad Complutense/Banco Santander (grant nº 921556) is gratefully thanked for financial support. L.C. thanks MINECO for a predoctoral scholarship (FPI, cofinanced by Fondo Social Europeo). Technical assistance from the ICTS Microscopy National Center (UCM) is acknowledged. The authors thank V. Martín and J. Sancho Franco for helping in sample preparation and measurement. The authors thank the reviewers for the careful analysis and rich comments that have helped to improve the final version of the manuscript.

Received: September 10, 2012
Revised: January 22, 2013
Published online: March 6, 2013

[1] D. S. Wiersma, *Nat. Phys.* **2008**, *4*, 359.
[2] H. Cao, Y. G. Zhao, S. T. Ho, E. W. Seelig, Q. H. Wang, R. P. H. Chang, *Phys. Rev. Lett.* **1999**, *82*, 2278.
[3] N. M. Lawandy, R. M. Balanchandran, A. S. L. Gomes, E Sauvain, *Nature* **1994**, *368*, 436.
[4] A. Costela, I. García–Moreno, L. Cerdán, V. Martín, O. García, R. Sastre, *Adv. Mater.* **2009**, *21*, 4163.
[5] C. Tolentino Domínguez, E. de Lima, P. C. de Oliveira, F. López Arbeloa, *Chem. Phys. Lett.* **2008**, *464*, 245.
[6] G. D. Dice, S. Mujumdar, A. Y. Elezzabi, *Appl. Phys. Lett.* **2005**, *86*, 131105.
[7] M. A. Noginov, *Solid-State Random Lasers*, Springer, New York **2005**.
[8] H. Noh, J.-K. Yang, S. F. Liew, M. J. Rooks, G. S. Solomon, H. Cao, *Phys. Rev. Lett.* **2011**, *106*, 183901.
[9] L. Sapienza, H. Thyrrestrup, S. Stobbe, P. D. García, S. Smolka, P. Lodahl, *Science* **2010**, *327*, 1352.
[10] S. K. Turitsyn, S. A. Babin, A. E. El-Taher, P. Harper, D. V. Churkin, S. I. Kablukov, J. D. Ania-Castañón, V. Karalekas, E. Podivilov, *Nat. Photonics* **2010**, *4*, 231.
[11] A. Tulek, R. C. Polson, Z. V. Vardeny, *Nat. Phys.* **2010**, *6*, 303.
[12] X. Zhao, Z. Wu, S. Ning, S. Liang, D. Wang, X. Hou, *Opt. Express* **2011**, *19*, 16126.
[13] a) L. Cerdán, A. Costela, G. Durán-Sampedro, I. García-Moreno, *Appl. Phys. B.* **2012**, *108*, 839. b) L. Cerdán, A. Costela, I. García-Moreno, *Org. Electron.* **2012**, *13*, 1463.
[14] X. H. Wu, A. Yamilov, H. Noh, H. Cao, E. W. Seelig, R. P. H. Chan, *J. Opt. Soc. Am. B* **2004**, *21*, 159.
[15] P. D. García, R. Sapienza, A. Blanco, C. López, *Adv. Mater.* **2007**, *19*, 2597.
[16] P. D. García, R. Sapienza, C. López, *Adv. Mater.* **2010**, *22*, 12.
[17] S. Gottardo, R. Sapienza, P. D. García, A. Blanco, D. S. Wiersma, C. López, *Nat. Photonics* **2008**, *2*, 429.
[18] Y. Chen, J. Herrnsdorf, B. Guilhabert, Y. Zhang, A. L. Kanobolotsky, P. Skabara, E. Gu, N. Laurand, M. D. Dawson, *Org. Electron.* **2012**, *13*, 1126.

[19] E. Enciso, A. Costela, I. García-Moreno, V. Martín, R. Sastre, *Langmuir* **2010**, *26*, 6154.
[20] V. Martín, J. Bañuelos, E. Enciso, I. López Arbeloa, A. Costela, I. García-Moreno, *J. Phys. Chem. C* **2011**, *115*, 3926.
[21] L. Cerdán, E. Enciso, V. Martín, J. Bañuelos, I. López-Arbeloa, A. Costela, I. García-Moreno, *Nat. Photonics* **2012**, *6*, 621.
[22] H. Cao, *J. Phys. A: Math. Gen.* **2005**, *38*, 10497.
[23] R. S. Farr, R. D. Groot, *J. Chem. Phys.* **2009**, *131*, 244104.
[24] C. Cabrillo, E. Enciso, M. J. Capitán, A. Cabañas, M. J. Torralvo, J. Alvarez, F. J. Bermejo, *Langmuir* **2011**, *27*, 2219.
[25] F. Rouquerol, J. Rouquerol, K. Sing, *Adsorption by Powders and Porous Solids*, Academic Press, London, UK **1999**.
[26] M. C. Carbajo, E. Climent, E. Enciso, M. J. Torralvo, *J. Colloid Interface Sci.* **2005**, *284*, 639.
[27] H. Cao, *Waves Random Media* **2003**, *13*, R1.
[28] J. Andreasen, A. A. Asatryan, L. C. Botten, M. A. Byrne, H. Cao, L. Ge, L. Labonté, A. D. Stone, H. E. Türeci, C. Vanneste, *Adv. Opt. Photon.* **2011**, *3*, 88.
[29] On-line Mie scattering Calculator by Scott Prahl, http://omlc.ogi.edu/calc/mie_calc.html (accessed February 2013).
[30] C. F. Bohren, D. R. Huffman, *Absorption and scattering of light by small particles*, Wiley-VCH, Weinheim, Germany **2004**.
[31] X. Wu, W. Fang, A. Yamilov, A. A. Chabanov, A. A. Asatryan, L. C. Botten, H. Cao, *Phys. Rev. A* **2006**, *74*, 053812.
[32] W. Holzer, A. Penzkofer, T. Schmitt, A. Hartmann, C. Bader, H. Tillmann, D. Raabe, R. Stockmann, H.-H. Hörnhold, *Opt. Quantum Electron.* **2001**, *33*, 121.
[33] F. Lahoz, C. J. Oton, N. Capuj, M. Ferrer-González, S. Cheylan, D. Navarro-Urrios, *Opt. Express* **2009**, *17*, 16766.
[34] S. John, G. Pang, *Phys. Rev. A* **1996**, *54*, 3642.
[35] L. Cerdán, A. Costela, I. García-Moreno, V. Martín, M. E. Pérez-Ojeda, *IEEE J. Quantum Electron.* **2011**, *47*, 907.
[36] I. Garcia Moreno, A. Costela, M. Pintado-Sierra, V. Martin, R. Sastre, *J. Phys. Chem. B* **2009**, *113*, 10611.
[37] I. Garcia Moreno, A. Costela, M. Pintado-Sierra, V. Martin, R. Sastre, *Adv. Funct. Mater.* **2009**, *19*, 2547.
[38] T. D. Nagao, N. Anzai, Y. Kobayashi, S. Gu, M. Konno, *J. Colloid Interface Sci.* **2006**, *298*, 232.
[39] J. W. Goodwin, R. H. Ottewill, R. Pelton, G. Vianello, D. B. Yates, *Br. Polym. J.* **1978**, *10*, 173.
[40] M. S. Tirumkudulu, W. B. Russel, *Langmuir* **2005**, *21*, 4938.